Available online at www.sciencedirect.com
ScienceDirect
Trans. Nonferrous Met. Soc. China 33(2023) 3198−3209
Transactions of Nonferrous Metals Society of China
www.tnmsc.cn

Arsenic extraction from copper concentrate using controlled oxidative roasting and filtration process

Xiao-wei TANG[1], Yue-hui HE[1,2]

1. Powder Metallurgy Research Institute, Central South University, Changsha 410083, China;
2. State Key Laboratory of Powder Metallurgy, Central South University, Changsha 410083, China

Received 28 October 2022; accepted 5 September 2023

Abstract: For more efficient treatment of arsenic-bearing copper concentrates, arsenic can be extracted in two steps: high-temperature filtration of dust and low-temperature separation of condensed arsenic oxide. The oxygen content in the roasting environment has an important effect on the residual arsenic content in the concentrate. When the oxygen content is high, the arsenate formed remains in the concentrate. When the oxygen content is low, the formation of arsenic sulphide can clog the filter cake residue. Roasting at 700 °C with an oxygen content of 4 vol.% results in the lowest residual arsenic content in the concentrate, from 11.8 to 0.34 wt.%. In the pilot experiment, the oxygen content was indirectly controlled by controlling the feed rate. The residual arsenic content is reduced to 0.48 wt.% and the purity of the recovered As_2O_3 reaches 99.17 wt.%. Based on the study of the mechanism of arsenic change with different oxygen contents, a new process of oxygen-controlled roasting is proposed and successfully applied in the pilot test, so that the residual arsenic content in copper concentrates is lower than the standard of arsenic content in imported minerals from China (0.5 wt.%).

Key words: arsenic; arsenic-bearing copper concentrate; filtration; roasting; porous material

1 Introduction

The depletion of high-grade ore has made copper deposits increasingly complex, leading to increased interest in the arsenic-contaminated resources [1−3]. Treating the arsenic copper concentrates using current copper smelting systems is a challenge due to the contamination of systems and difficulty in separation and recovery. Hence, the arsenic-contaminated concentrates require pretreatment for initial arsenic separation, especially for enargite [4,5] and tennantite [6,7]. The arsenic content of the smelting system feed should not exceed 0.5 wt.% [8]. The literature offers several strategies for pretreatment, though there are many problems. For example, hydrometallurgy [9,10] and biometallurgy [11,12] can lead to arsenic entering solutions, resulting in ineffective separation and wastewater treatment. Pyrometallurgy [13,14], with its high efficiency, is used in industries and can be divided into two categories. The first is direct fixation of arsenic as calcium arsenate through lime roasting [15] or soda roasting [16,17]. The second is volatilization of arsenic to sulfides or oxides with other fugitive via oxidation roasting [18,19], neural roasting [20], and reduction roasting [21,22]. These flue gases need to be collected and treated in secondary processes, such as roasting or leaching, but this two-step treatment process is long and energy-intensive.

To solve these problems, we suggest combining two steps for the fabrication of solid arsenic oxide in situ: complete volatilization of arsenic into gaseous oxide via controlled oxidative roasting, followed by filtration of high-temperature

Corresponding author: Yue-hui HE, E-mail: yuehui@csu.edu.cn
DOI: 10.1016/S1003-6326(23)66327-7

gas in the flue gas collection to condense out the arsenic oxide. Porous intermetallic materials are used for the first step of filtration due to their excellent sulfidation resistance and high-temperature mechanical properties [23−26]. This approach offers various advantages, such as short process duration, low energy consumption, high separation efficiency, elimination of arsenic contamination from the source, no arsenic leakage, as well as direct preparation of high purity arsenic trioxide. However, arsenic displays erratic behavior during the roasting with several different condensed/gaseous oxides and sulfides formed. Concretely, a low oxygen content causes the generation of arsenic trisulfide with a high boiling point, resulting in filter membrane blockage. A high oxygen content leads to non-volatile arsenate generation. Therefore, the key to ensuring high separation efficiency and proper filtration process lies in the control of the formation and volatilization of gaseous arsenic oxide in the roasting process.

In this work, a one-step process for direct separation and extraction of arsenic was proposed. It involves filtering dust containing arsenic oxide obtained from copper−arsenic concentrates roasting to produce solid arsenic trioxide in situ. The thermodynamic and kinetic analysis was used to analyze the feasibility of the controlled oxidative roasting and experiments were conducted to determine optimal conditions. Pilot tests were also conducted to verify the filtration process, providing a new perspective for efficient arsenic extraction.

2 Experimental

2.1 Materials

The arsenic-containing copper concentrate used in this work was provided by the Aluminum Corporation of China (CHINALCO). The chemical components were characterized by inductive coupled plasma (ICP) and shown in Table S1 in Supporting materials (SM), and its main chemical components are Cu (23.2 wt.%), Fe (23.4 wt.%), S (34.8 wt.%), and As (11.8 wt.%). The mineral compositions were characterized by X-ray diffraction (XRD) and shown in Fig. S1 in SM. Determination of specific content adopted the *K* value method with adding Al_2O_3 as standard sample which was calculated by the following formula:

$$I_x/I_s=K_xW_x/W_s \quad (1)$$

where I is the diffraction intensity, K is the reference intensity ratio (RIR), W is the mass fraction, "x" means the measuring sample, and "s" means the standard sample (Al_2O_3). As shown in Table S2 in SM, the ratio of main mineral composition is tennantite (Cu_3AsS_3, 49.26 wt.%), chalcopyrite ($CuFeS_2$, 33.80 wt.%) and pyrite (FeS_2, 16.94 wt.%).

2.2 Thermodynamic approaches

The thermodynamic analysis was performed using the equilibrium composition module in HSC Chemistry® 6.0. The thermodynamic data of specific substances are listed in Table S3 in SM, which were obtained from database module of HSC and CRC Handbook of Chemistry and Physics (Internet Version 2016). According to literature and mechanism analysis, the substances that may be produced during the roasting process were divided into gases and solids. And the initial amount of thermodynamic equilibrium was determined by the mineralogical composition calculation corresponding to 1000 kg of concentrate and the results are also shown in Table S3 in SM.

2.3 Kinetics approaches

The roasting of concentrate was a gas−solid reaction and the kinetics was analyzed by the following three-dimensional diffusion rate equation:

$$1-(1-r)^{1/3}=kt \quad (2)$$

with

$$r=(m_0-m_t)/m_0 \quad (3)$$

where r is the fractional conversion, k is the apparent rate constant, m_0 is the initial mass of the concentrate sample, and m_t is the mass at time t.

The dependence of the rate constant on the temperature is given by

$$k=A\exp[-E/(RT)] \quad (4)$$

where A is the preexponential factor, E is the activation energy, R is the molar gas constant, T is the thermodynamic temperature.

2.4 Specific surface area calculation

The BET adsorption isotherm was used to calculate the specific surface area. The adsorption isotherm equation is shown in Eq. (5):

$$\frac{P}{V[(P_0-P)-1]}=\frac{1}{CV}+\frac{C-1}{CV}\frac{P}{P_0} \quad (5)$$

where P is the actual pressure of the adsorbate at the adsorption temperature, P_0 is the saturated vapor pressure of the adsorbate at the adsorption temperature, V is monolayer saturated adsorption capacity, and C is a constant. According to the slope (s) and intercept (M) of the curve, the adsorption amount V of forming the monomolecular layer is obtained as

$$V=1/(s+M) \quad (6)$$

Finally, the specific surface area was calculated by

$$S=S_A NV/(2.2414\times10^{22}) \quad (7)$$

where S_A is average cross-sectional area of each adsorbed molecule, and N is Avogadro's constant.

2.5 Experimental method

The schematic diagram of the roasting setup is presented in Fig. 1(a). The air was pumped into the gas mixing system through a peristaltic pump and mixed with nitrogen. The mixed gas was divided into two parts: one part entered the gas detector for oxygen content detection, and the other part entered the tube furnace under the control of the gas flow meter. For each experiment, copper concentrate with required mass was placed at a crucible in the furnace and heated to the desired temperature. A piece of glass was placed behind the insulation to collect condensate volatilized from the concentrate. Gas was discharged after being purified by NaOH solution.

The pilot experiments were conducted in a rotary furnace, and the supporting equipment was shown in Fig. 1(b). The concentrate was charged into the rotary furnace through the driving of the motor and decomposed into arsenic-containing smoke and cleaner concentrate. The heat of the decomposition process was provided by the combustion of diesel in the combustion chamber, where the outer wall of rotary furnace was heated to rise the temperature. To remove dust, arsenic-containing gas was delivered to the filter. Finally, dust-free arsenic gas entered the arsenic recovery system.

2.6 Characterization

The content of the solids was measured by inductively coupled plasma-atomic emission spectrometry (ICP-OES, 7200, Thermal Electron Corporation, USA) after acid leaching (aqua regia). The phase of the solids was determined by X-ray diffraction (XRD, Empyrean 2, PA Nalytical, Netherlands) using Cu K_α radiation at a scanning rate of 15 (°)/min. The decomposition reaction of concentrates in air was gained from the thermogravimetric analysis (TG) and differential thermal analysis (DTA). The specific surface area and pore size of the concentrates were evaluated by the BET method.

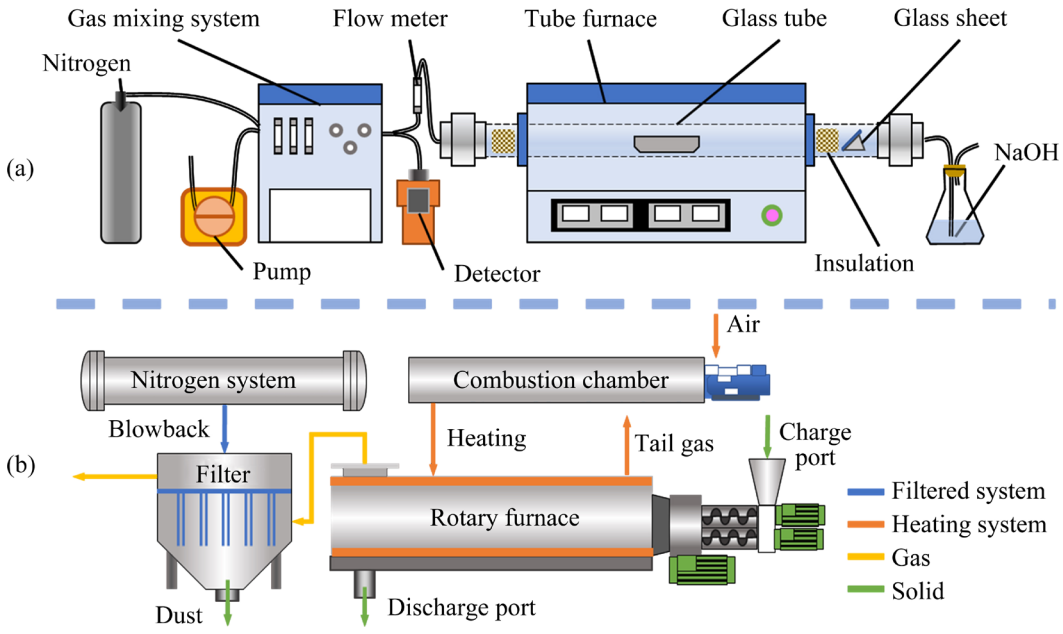

Fig. 1 Roasting experimental setup (a) and pilot-scale experiment equipment (b)

3 Results and discussion

3.1 Reaction mechanism

The samples were heated to a maximum temperature of 1000 °C in the TG and DTA experiments (Fig. 2(a)). Due to the high sulfur content of the concentrate, it could not be directly used for detection. 9 times the mass of Al_2O_3 was added to the concentrate to dilute the concentration. However, this method did not affect the test results. The DTA curve of the concentrate exhibited temperature peak at 95.72 and 497.49 °C. The temperature peaks were the boiling points of water and sulfur, respectively. The TG curve of the concentrate exhibited temperature change in four stages. Meanwhile, in Fig. 2(b), the material components of these four stages were detected by XRD. By comparing the components at 300, 500, 600, and 750 °C, the reaction mechanism was deduced as follows.

In the first stage, moisture in the concentrate started to volatilize. In the second stage, arsenic-containing copper concentrate was decomposed during heating. The specific reaction process was reported by NAKAZAW et al [27] that enargite is oxidized at 193−550 °C by Reaction (8) and PADILLA et al [19] reported that enargite transformation to tennantite starts at 550 °C by Reactions (9) and (10):

$$4Cu_3AsS_4(s)+13O_2=6Cu_2S(s)+As_4O_6(g)+10SO_2(g) \quad (8)$$

$$4Cu_3AsS_4(s)=Cu_{12}As_4S_{13}(s)+1.5S_2(g) \quad (9)$$

$$Cu_{12}As_4S_{13}(s)=6Cu_2S(s)+2As_2S_3(g)+0.5S_2(g) \quad (10)$$

Also, the decomposition of chalcopyrite and pyrite was reported by CHAKRABORTI and LYNCH [28], outlined in the following reactions:

$$4CuFeS_2(s)=4FeS(s)+4CuS(s) \quad (11)$$

$$2FeS_2(s)=2FeS(s)+S_2(g) \quad (12)$$

In the third stage, the oxidized substance formed hard-to-volatile sulfate as the following reactions:

$$CuS(s)+2O_2(g)=CuSO_4(s) \quad (13)$$

$$FeS_2(s)+O_2(g)=3Fe_2(SO_4)_2(s)+SO_2(g) \quad (14)$$

In the fourth stage, sulfate decomposition occurred in following reaction:

$$2CuSO_4(s)=2CuO(s)+SO_2(g)+O_2(g) \quad (15)$$

$$2Fe_2(SO_4)_2(s)=2Fe_2O_3(s)+6SO_2(g)+3O_2(g) \quad (16)$$

In addition, a small amount of iron arsenate was formed although the content of iron arsenate was too low to detect in XRD pattern. The reaction was shown as follows [29]:

$$4FeAsO_4(s)=2Fe_2O_3(s)+As_4O_6(g) \quad (17)$$

As show in Fig. 3, the trend of arsenic was the main research object. The complex reaction process

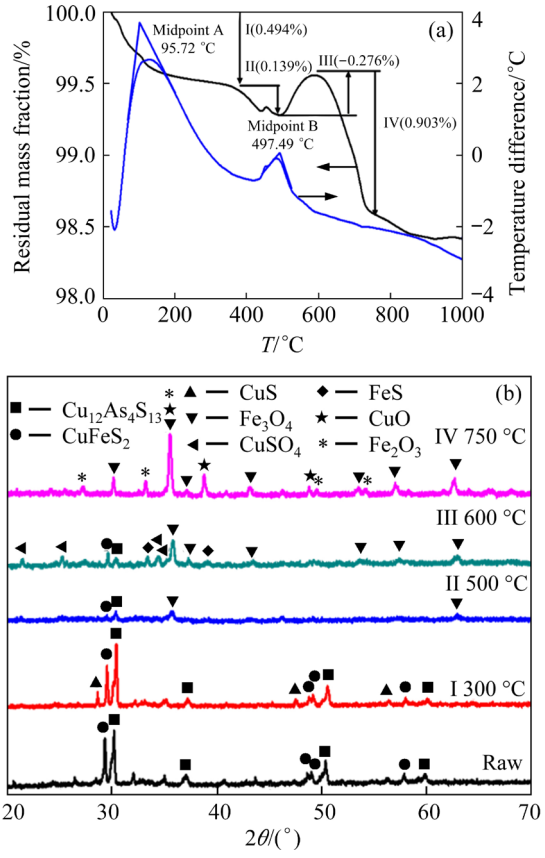

Fig. 2 TG and DTA curves of concentrate decomposition in air (a) and XRD patterns of concentrate decomposition in different stages (b)

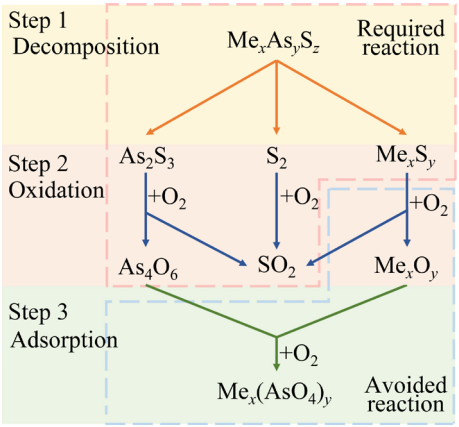

Fig. 3 Mechanism of decomposition process of concentrates

above was roughly divided into three steps: (1) decomposition, (2) oxidation, and (3) adsorption. In the roasting process, the decomposition of $Me_xAs_yS_z$ and the oxidation of As_2S_3 were required. Conversely, the oxidation of Me_xO_y and the recombination of $Me_x(AsO_4)_y$ needed to be avoided.

3.2 Thermodynamic analysis

Thermodynamic calculations were performed based on the reaction mechanism. Figure 4(a) shows the changes in the reaction amounts of all the possible compounds involved in roasting at different temperatures and oxygen amounts. Next, Fig. 4(b) extracts the arsenic-containing compounds to form a new equilibrium diagram. And it was found that there was a part of the region that had neither arsenic sulfide nor arsenate. For a more intuitive result, it is necessary to observe Fig. 4(b) in two directions (z–y plane and x–y plane). Figure 4(c) shows the equilibrium diagram at 700 °C, corresponding to the z–y plane of Fig. 4(b). Arsenic was divided into three ranges of arsenic sulfide, arsenic oxide, and arsenate, as shown in Parts I, II, and III, respectively. In general, to obtain pure arsenic oxide in Part II, the oxygen amount was controlled to be 5−10 kmol. Figure 4(d) shows the equilibrium diagram in zero equilibrium amount, corresponding to x–y plane of Fig. 4(b). In Fig. 4(d), the blank part was found when the oxygen amount was 5−10 kmol and temperature was above 550 °C. However, the reaction took time during the actual process, and the oxygen was equilibrated during the reaction while maintaining a specific oxygen potential. Further kinetic calculations and conditional experiments of oxygen potential were required.

3.3 Kinetics analysis

In Fig. 5(a), the kinetic experiments were conducted from 600 to 800 °C. It can be found that the curve shape converged after the temperature exceeded 700 °C. In Fig. 5(b) and Table 1, the fractional conversion r was linearly fitted to time after conversion with the reaction rate equation. Linear fit was very high below 650 °C. And linear fit above 700 °C was clearly divided into two periods, because the volatilization of arsenic sulfate on the surface was in the form of three-dimensional diffusion, but the internal sulfuric arsenic was affected by the form of pore obstruction diffusion.

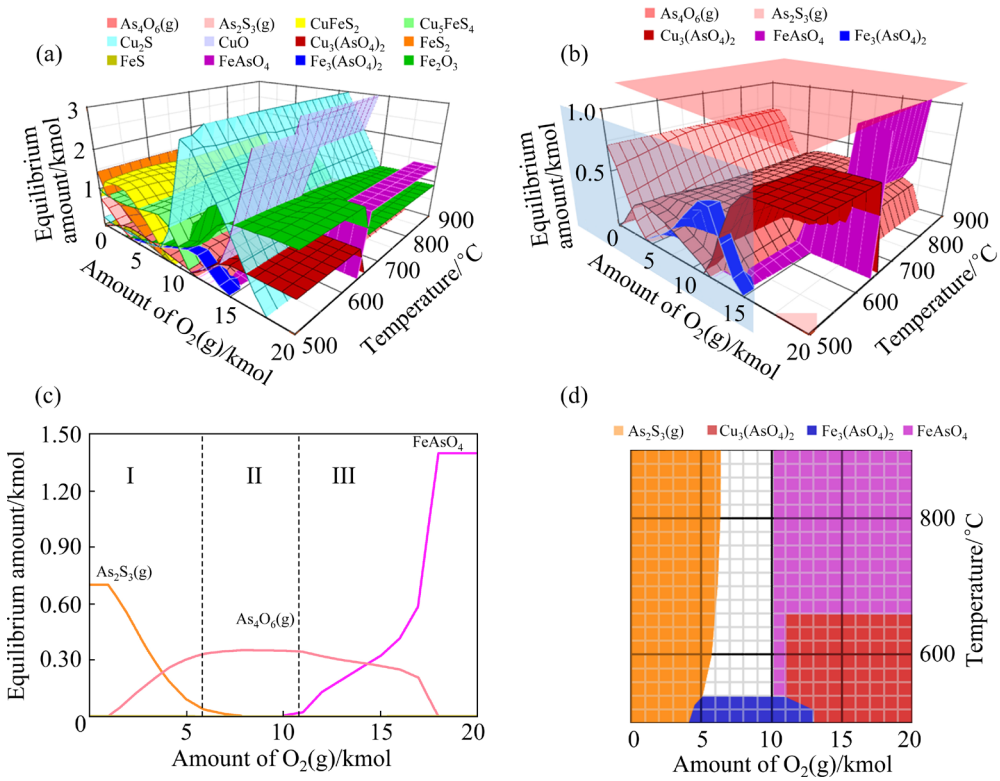

Fig. 4 3D thermodynamic equilibrium diagrams of possible compositions (a) and arsenic-containing compositions (b); Cross section of equilibrium diagram over temperature (c); Distribution of arsenic-containing compositions on cross section of equilibrium amount (d)

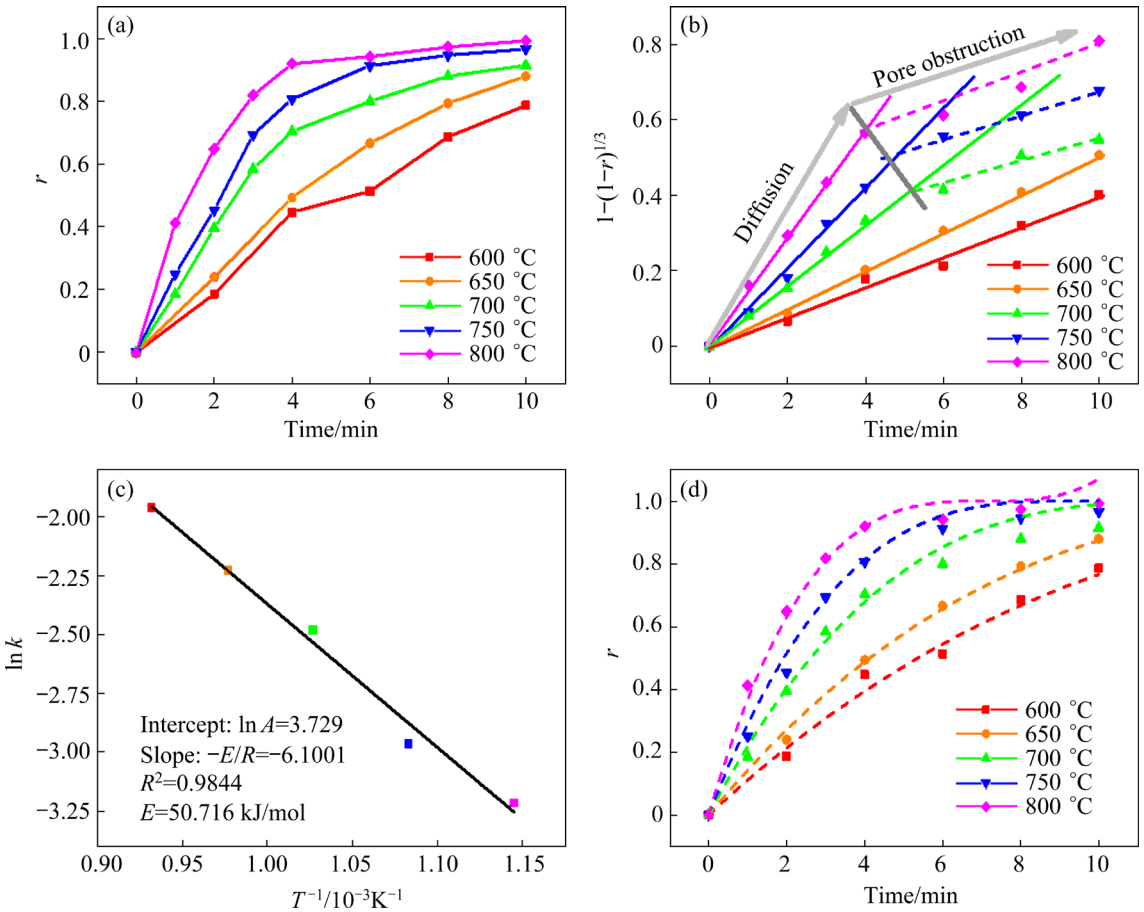

Fig. 5 Changes of fractional conversion with time (a); Linear fitting of reaction rate equation and time (b); Linear fitting of ln k and $1/T$ (c); Validation of fitted equations (d)

Table 1 Rate constants for roasting of concentrate

Temperature/°C	$T^{-1}/10^{-3}$ K^{-1}	k	ln k	R^2
600	1.145	0.0401	−3.21638	0.987
650	1.083	0.0515	−2.96617	0.998
700	1.027	0.0837	−2.48052	0.997
750	0.977	0.1078	−2.22748	0.990
800	0.932	0.1406	−1.96184	0.998

Thus, only the diffusion part was considered for the fit above 700 °C. The value of activation energy was obtained as 50.716 kJ/mol by linearly fitting the results k and the reciprocal of time for the fit at different temperatures in Fig. 5(c). The activation energy of the process was calculated according to the Arrhenius diagrams and the kinetic equation for roasting of concentrate was found to be

$$1-(1-r)^{1/3}=41.637t\cdot\exp(-6100/T) \quad (18)$$

From Eq. (18), the time to reach the desired fractional conversion may be estimated. Finally, the fitting equation and the actual reaction data were compared in Fig. 5(d) due to the pore obstruction of concentrate after 10 min. The equation fitted well in the early periods, but poor in the later periods.

3.4 Effect of oxygen potential

The XRD patterns of volatiles condensed in different roasting oxygen potentials are shown in Fig. 6(a), and the main volatile was As_4O_6 at the partial pressure of oxygen of 4.052−8.104 kPa. However, As_4S_4 started to generate when the partial pressure of oxygen was lower than 2.026 kPa. The formation of As_4S_4 had an adverse effect on subsequent filtering. Therefore, the partial pressure of oxygen during roasting should not be lower than 2.026 kPa. Figure 6(b) shows XRD pattern of roasted concentrate in different oxygen partial pressures. $CuFeS_2$ was gradually decomposed and Fe_3O_4 was constantly generated with the increase of oxygen partial pressure, which was not conducive to the preservation of sulfur. The addition of carbon also reduced the oxygen partial pressure. Figure 6(c)

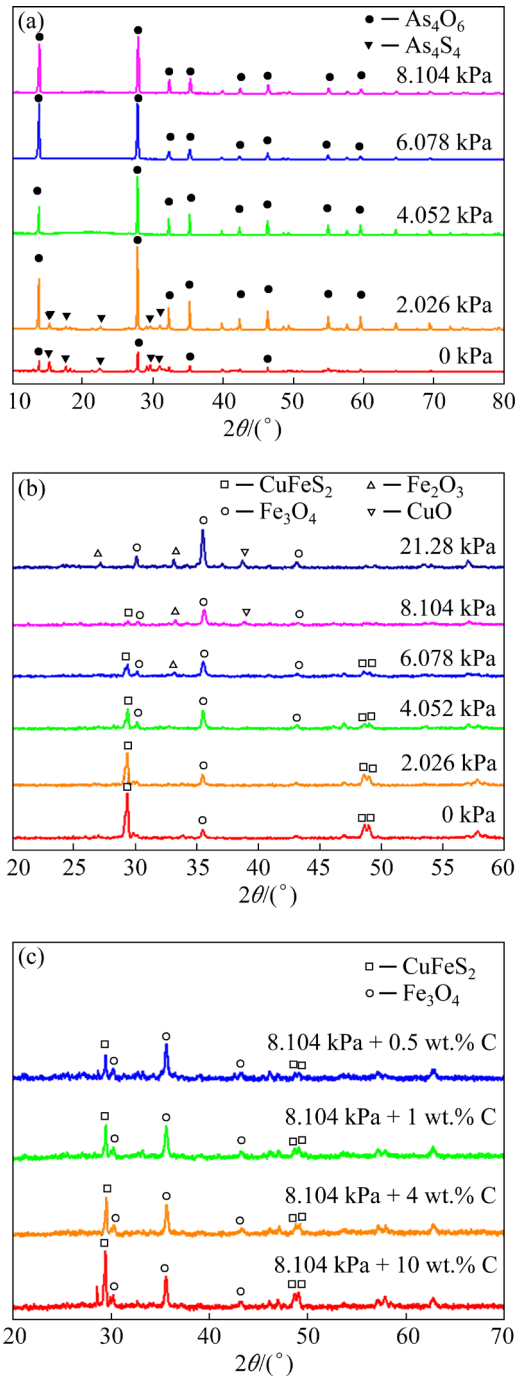

Fig. 6 XRD pattern of volatiles condensed (a), roasted concentrate with different oxygen partial pressures (b), and roasted concentrate with different carbon contents added (c)

shows XRD pattern of roasted concentrate with different contents of carbon added. It was observed that the increase of carbon content was accompanied by an increase of $CuFeS_2$ content, which indicated that the increase of carbon content reduced the decomposition of $CuFeS_2$. The process with different contents of carbon added was similar to the process of different partial pressures of oxygen, which indicated that the increase of carbon content could indirectly reduce the oxygen partial pressure during the roasting of concentrates.

3.5 Effect of additives

The isotherm adsorption and desorption curves were drawn. Figure 7(a) shows the isotherm adsorption and desorption curves of concentrate. In Fig. 7(b), the roasted concentrate without additives had separate adsorption and desorption curves and a distinct hysteresis loop was formed. The formation of hysteresis loops of this shape indicated that there were bottleneck-shaped holes in roasted concentrate. The formation of such pores caused the adsorption volume to be larger than the desorption volume under the same pressure, which was not conducive to the volatilization of arsenic in the subsequent pores. However, with the addition of sand and carbon in Figs. 7(c, d), the hysteresis loop became a cylindrical shape, which was beneficial to the volatilization of arsenic during concentrate roasting.

Since the isotherm in Fig. 7 belonged to Type IV in the Brunauer classification, the BET adsorption isotherm was used to calculate the specific surface area. And the calculation result is shown in Fig. S2 in SM, and the specific surface area was 0.913 m^2/g for concentrate, 0.484 m^2/g for direct roasted concentrate, 0.590 m^2/g for roasted concentrate with sand, and 2.457 m^2/g for roasted concentrate with carbon. The direct roasted concentrate had a smaller specific surface area, which was another reason why arsenic was difficult to volatilize. When sand and carbon were added, the specific surface area increased, and the increased specific surface area was more conducive to the volatilization of arsenic.

3.6 Optimizing conditions

The optimizing conditions during roasting experiment was explored. The experimental conditions are given in Table S4 in SM and the experimental procedure was carried out in the order of temperature, time, oxygen content, and flow rate, and finally the addition of carbon and sand was additionally investigated.

In Fig. 8(a), the residual arsenic content decreased rapidly as the temperature increased from 500 to 700 °C. Then, as the temperature continued to increase, the decline in arsenic removal slowed

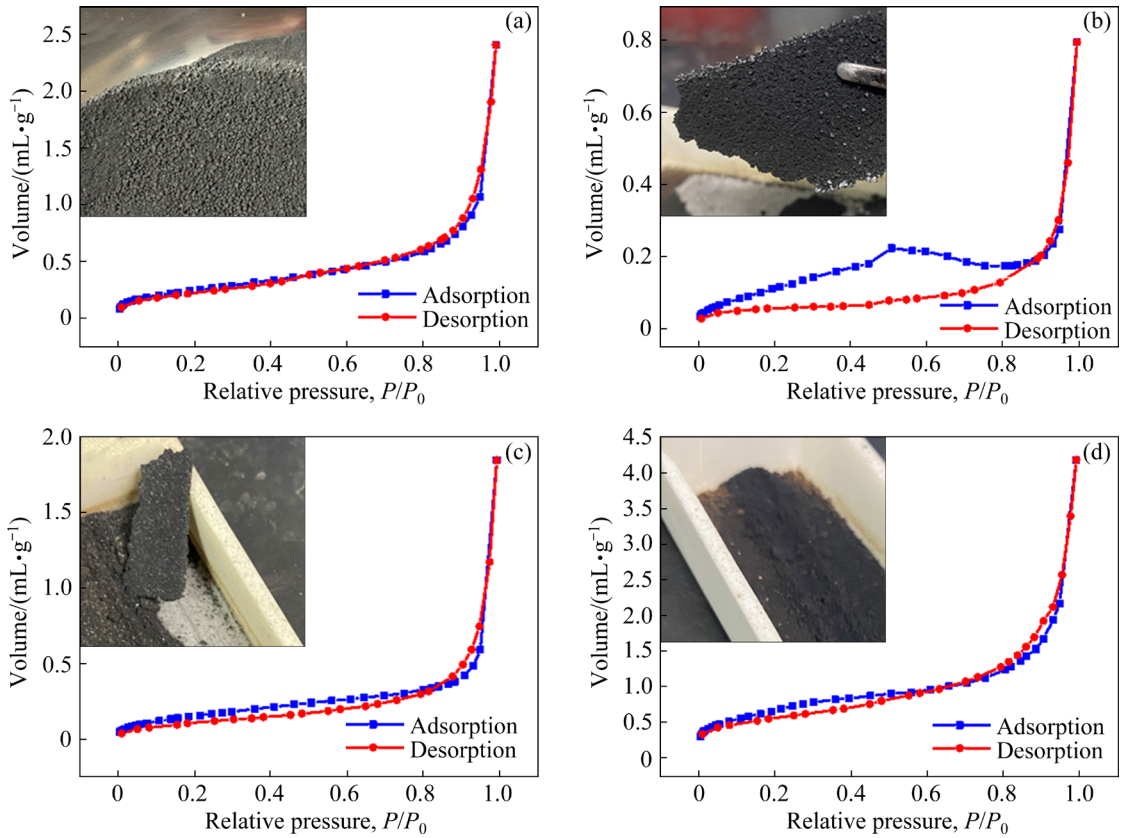

Fig. 7 Isotherm adsorption and desorption curves of concentrate (a), roasted concentrate (b), roasted concentrate with sand (c), and roasted concentrate with carbon (d)

down, but the loss of sulfur increased rapidly. The residual arsenic content decreased to 0.77 wt.% when the temperature was 700 °C. In Fig. 8(b), the residual arsenic content was minimized at 30 min, and most of the arsenic in the concentrate was removed. However, when the time was extended to 60 min, the amount of residual arsenic increased because magnetite was produced, and arsenic-containing gas in furnace was not completely discharged. The residual arsenic content was minimized to 0.39 wt.% at 30 min. In Fig. 8(c), the arsenic content had slight fluctuations in the oxygen content range of 0−4 vol.% and decreased to a minimum of 0.39 wt.% at an oxygen content of 4 vol.%. In contrast, the arsenic content increased as the oxygen content increased from 4 to 8 vol.%. In Fig. 8(d), the residual arsenic content had minimal variation when gas flow rate was between 0.2 and 0.6 L/min, which meant that considerably less gas entered the system than the gas volatilized from the concentrate itself. However, the arsenic content decreased when the flow rate increased to 0.8 L/min because the arsenic volatilized from the concentrate was quickly removed by the gas flow.

SiO_2 (sand) and C (carbon) were added to prevent residual arsenic caused by the accumulation of small concentrate particles. To observe the effect of additives more clearly, the additive effect experiments were conducted at 650 °C. As shown in Fig. 8(e), the residual arsenic content was reduced by the addition of SiO_2. However, the residual arsenic content was unchanged when the SiO_2 content increased from 8 to 12 wt.%. Because 5 g of SiO_2 was sufficient to create suitable gaps for arsenic volatilization, in Fig. 8(f), the residual arsenic content decreased continuously with the addition of small amounts of C.

3.7 Pilot-scale experimental results

The main conditions and results of the pilot plant experiments are given in Table 2. The pilot experiment was divided into three stages according to the purpose of the experiment. The first stage (No. 1−3) was to adjust the temperature of the equipment above 700 °C in the pre-experiment. In this stage, reducing the feed rate was beneficial to the removal of arsenic. In the second stage (No. 3−8), the feed rate was reduced to 50 kg/h.

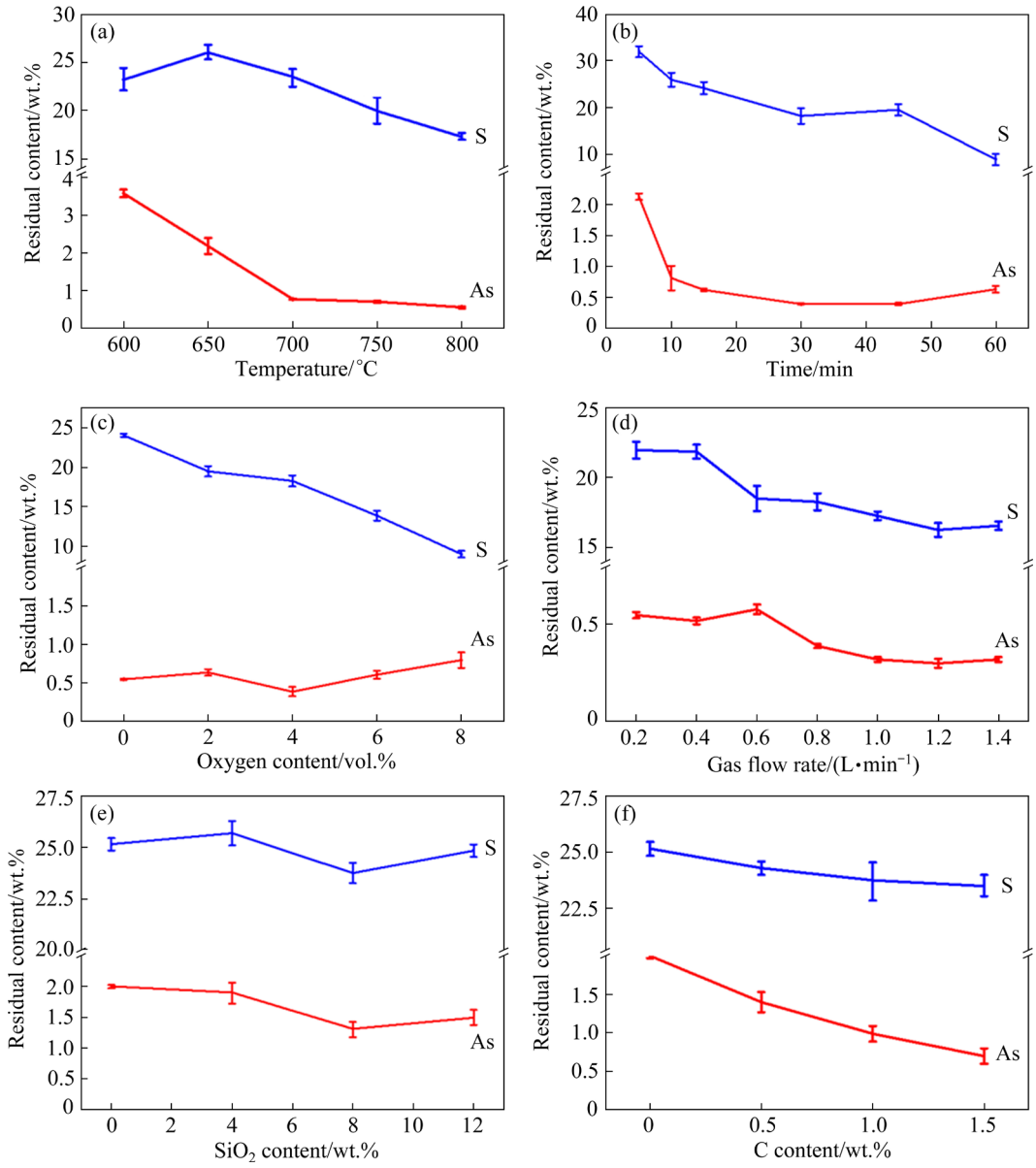

Fig. 8 Effect of temperature (a), time (b), oxygen content (c), gas flow rate (d), SiO_2 content (e), and carbon content (f) on sulfur and arsenic residual content

Table 2 Results of pilot plant experiment

No.	Sand content/wt.%	Carbon content/wt.%	Feeding rate/ (kg·h^{-1})	Temperature/ °C	Arsenic removal rate/%	Remaining arsenic content/wt.%
1	10	0	200	690−740	92.50	0.83
2	10	0	100	670−740	92.87	0.78
3	10	2	100	700−740	93.24	0.74
4	10	2	50	750−760	47.62	5.73
5	10	2	50	780−800	62.16	4.14
6	10	3	50	760−810	70.20	3.26
7	10	3	50	730−760	73.13	2.97
8	10	3	50	700−750	72.03	3.06
9	10	3	100	700−740	94.51	0.60
10	10	3	120	700−740	93.98	0.66
11	10	3	80	700−740	95.61	0.48

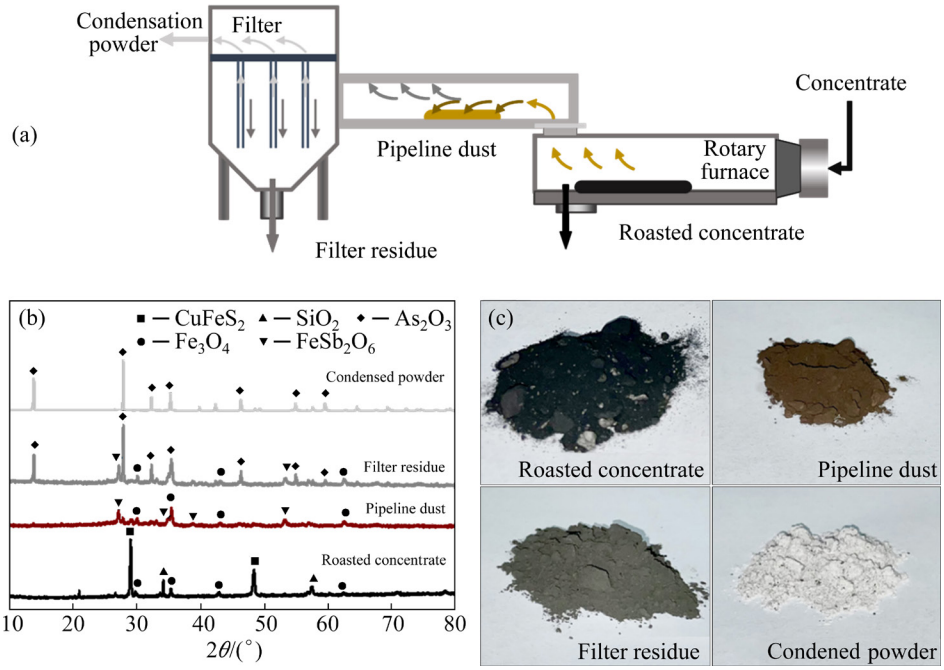

Fig. 9 Output route of solid products (a); XRD patterns of solid product (b); Photos of solid products (c)

However, because the reduction in the feed rate relatively increased the oxygen content in the roaster, difficult-to-volatilize substances, such as iron arsenate, were produced. Therefore, other adjustments to the process were ineffective. In the third stage (No. 9−11), the feed rate was increased to 100 kg/h and then adjusted. When the feed rate was adjusted to 80 kg/h, the residual arsenic content was reduced to 0.48 wt.%, which met the Chinese National Import Standard. This indicated that the oxygen content in the roasting environment can be indirectly controlled by adjusting the feed rate.

In Fig. 9(a), the solid components of discharge port, pipeline, filter residue outlet, and filter gas outlet during the filtration process were studied, and the main components are shown in Fig. 9(b). The main components of the roasted concentrate were $CuFe_2S_3$, Fe_3O_4, and SiO_2, which were directly used in the subsequent copper smelting system. The main components of the pipeline dust were Fe_3O_4, and $FeSb_2O_4$. This part of the dust was carried out to form the rotary furnace by the hot air flow and then accumulated in the pipe, which was easy to cause blockage of the pipe. This problem was solved by adjusting the pipe angle. The main components of the filter residue were Fe_3O_4, $FeSb_2O_4$, and As_2O_3. The existence of As_2O_3 was due to the clogging of the filter, and increasing the frequency of backflushing could solve the problem. The arsenic content of the condensed powder could reach 99.17 wt.% which could be directly used as a product.

Based on the above results, a novel process for arsenic extraction of arsenic-containing copper concentrate was proposed, as shown in Fig. 10. This process consisted of two steps: one was high-temperature filtration to remove dust, and the other was low-temperature filtration to collect white arsenic. Through oxygen-controlled roasting technology, arsenic was extracted and recycled in the form of arsenic trioxide. Finally, the process realized the arsenic-free treatment of arsenic-containing copper concentrate and the white arsenic could be directly used as a product. The whole scheme achieved efficient and economical disposal of arsenic-containing copper concentrate.

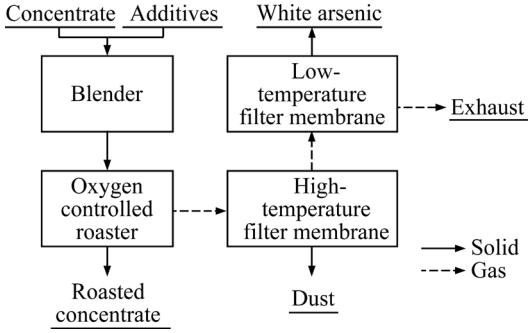

Fig. 10 Technical scheme for arsenic extraction from arsenic-containing concentrate

4 Conclusions

(1) In the thermodynamic analysis, the feasibility of controlled oxidative roasting was determined, and a roasting temperature above 700 °C was proven to be suitable for roasting. In the laboratory experiments, the roasting kinetic formula was proposed as $1-(1-r)^{1/3}=41.637t\cdot\exp(-6100/T)$.

(2) The effect of oxygen partial pressure was explored, and the positive effects of the additives, sand and carbon, were confirmed. The optimal roasting conditions was concluded to be roasting temperature of 700 °C, roasting time of 30 min, roasting flow rate of 1 L/min, and roasting oxygen content of 4 vol.%. In the pilot tests, the arsenic content of the concentrate was reduced to 0.48 wt.% at a charging rate of 80 kg/h. In addition, the arsenic trioxide content recovered after filtration was 99.17 wt.%. The process achieved the arsenic-free treatment of concentrates and direct fabrication of the white arsenic as a product. This provided a new perspective for efficient arsenic extraction in arsenic-bearing copper concentrate.

Supporting materials

Supporting materials in this paper can be found at: http://tnmsc.csu.edu.cn/download/23-p3198-2022-1224-Supporting_Materials.pdf.

References

[1] RTZER N, SCHMIDT M. Historical, current, and future energy demand from global copper production and its impact on climate change [J]. Resources, 2020, 9(4): 44.

[2] VILLENA M, GREVE F. On resource depletion and productivity: The case of the Chilean copper industry [J]. Resources Policy, 2018, 59: 553−562.

[3] DONG D, OERS L V, TUKKER A, van der VOET E. Assessing the future environmental impacts of copper production in China: Implications of the energy transition [J]. Journal of Cleaner Production, 2020, 274: 122825.

[4] LATTANZI P, da PELO S, MUSU E, ATZEI D, ELSENER B,FANTAUZZI M, ROSSI A. Enargite oxidation: A review [J]. Earth Science Reviews, 2008, 86(1/2/3/4): 62−88.

[5] PLACKOWSKI C, NGUYEN A V, BRUCKARD W J. A critical review of surface properties and selective flotation of enargite in sulphide systems [J]. Minerals Engineering, 2012, 30: 1−11.

[6] PETRUS H T, HIRAJIMA T, SASAKI K, OKAMOTO H. Effects of sodium thiosulphate on chalcopyrite and tennantite: An insight for alternative separation technique [J]. International Journal of Mineral Processing, 2012, 102: 116−123.

[7] SACK R O. Thermochemistry of tetrahedrite−tennantite fahlores [M]//The Stability of Minerals. London: Chapman & Hall, 1992: 243−266.

[8] LIU X T, SUN J. Copper ore trade and quality inspection [M]. Jinan: China Ocean University Press, 2016: 148−149. (in Chinese)

[9] SAFARZADEH M S, MOATS M S, MILLER J D. Evaluation of sulfuric acid baking and leaching of enargite concentrates [J]. Minerals & Metallurgical Processing, 2012, 29(2): 97−102.

[10] SAFARZADEH M S, MOATS M S, MILLER J D. Acid bake-leach process for the treatment of enargite concentrates [J]. Hydrometallurgy, 2012, 119−120: 30−39.

[11] AI C, MCCARTHY S, LIANG Y, RUDRAPPA D, QIU G, BLUM P. Evolution of copper arsenate resistance for enhanced enargite bioleaching using the extreme thermoacidophile *Metallosphaera sedula* [J]. Journal of Industrial Microbiology & Biotechnology, 2017, 44(12): 1613−1625.

[12] ELKINA Y A, MELNIKOVA E A, MELAMUD V S, BULAEV A. Bioleaching of enargite and tennantite by moderately thermophilic acidophilic microorganisms [J]. Microbiology, 2020, 89(4): 413−424.

[13] SAFARZADEH M S, MILLER J D. The pyrometallurgy of enargite: A literature update [J]. International Journal of Mineral Processing, 2016: 103−110.

[14] TAYLOR P R, PUTRA T A R. Pyrometallurgical processing technologies for treating high arsenic copper concentrates [M]. Springer, Cham: Celebrating the Megascale, 2014: 197−211.

[15] BARTLETT R W, HAUNG H H. Fluidized bed roasting of lime copper concentrate pellets [J]. Metallurgical Transactions B, 1976, 7(3): 489−490.

[16] LIU J, CHI R, XU Z, ZENG Z, LIANG J. Selective arsenic-fixing roast of refractory gold concentrate [J]. Metallurgical & Materials Transactions B, 2000, 31: 1163−1168.

[17] CHAMBERS B, PICKLES C A, PEACEY J G. Thermodynamic analysis of the sulphation roasting of enargite concentrates [J]. High Temperature Materials & Processes, 2012, 31(4/5): 613−625.

[18] KIM B S, KIM E Y, KIM C K, LEE H I, SOHN J S. Kinetics of oxidative roasting of complex copper concentrate [J]. Materials Transactions, 2008, 49(5): 1192−1198.

[19] PADILLA R, ARACENA A, RUIZ M C. Reaction mechanism and kinetics of enargite oxidation at roasting temperatures [J]. Metallurgical & Materials Transactions B, 2012, 43: 1119−1126.

[20] WILKOMIRSKY I, PARRA R, PARADA F, BALLADARES E. Mineralochemical characterization of calcines and flue dusts during neutral roasting of arsenic copper concentrates in the pilot plant of University of Concepción [C]//Conference of Metallurgists Proceedings. Westmount, Canada: Canadian Institute of Mining, Metallurgy and Petroleum, 2014.

[21] LI Y G. The study of reduction roasting-ammonia leaching of a low grade copper oxide ore [J]. Multipurpose Utilization of Mineral Resources, 2000(6): 7−10. (in Chinese)

[22] WAN X Y, QI Y H, GAO J J. New technique for removing arsenic from arsenic-containing copper slag by reduction−roasting in N_2−CO atmosphere [J]. Mining and Metallurgical Engineering, 2017, 37(6): 80−83.
[23] JIANG Y, HE Y, LIU C T. Review of porous intermetallic compounds by reactive synthesis of elemental powders [J]. Intermetallics, 2018, 93: 217−226.
[24] GAO H, HE Y, SHEN P, ZOU J, XU N, JIANG Y, LIU C T. Porous FeAl intermetallics fabricated by elemental powder reactive synthesis [J]. Intermetallics, 2009, 17: 1041− 1046.
[25] SHENG P Z, GAO L, GAO H Y, HE Y. High-temperature sulfidation behavior and application in SO_2-containing gas cleanup of porous FeAl intermetallics [J]. Materials Science and Engineering of Powder Metallurgy, 2010, 15(1): 38−43. (in Chinese)
[26] ZHANG H, LIU X, JIANG Y, GAO L, YU L, LIN N, LIU C T. Direct separation of arsenic and antimony oxides by high-temperature filtration with porous FeAl intermetallic [J]. Journal of Hazardous Materials, 2017, 338: 364−371.
[27] NAKAZAW S, YAZAWA A, JORGENSEN F. Simulation of the removal of arsenic during the roasting of copper concentrate [J]. Metallurgical & Materials Transactions B, 1999, 30: 393−401.
[28] CHAKRABORTI N, LYNCH D C. Thermodynamics of roasting arsenopyrite [J]. Metallurgical Transactions B, 1983, 14(2): 239−251.
[29] WILKOMIRSKY I, PARRA R, PARADA F, BALLADARES E, SEGUEL E, ETCHEVERRY J, DÍAZ R. Thermodynamic and kinetic mechanisms of bornite/ chalcopyrite/magnetite formation during partial roasting of high-arsenic copper concentrates [J]. Metallurgical & Materials Transactions B, 2020, 51: 1540−1551.

采用控制氧化焙烧过滤法从铜精矿中提取砷

唐晓威[1]，贺跃辉[1,2]

1. 中南大学 粉末冶金研究院，长沙 410083；
2. 中南大学 粉末冶金国家重点实验室，长沙 410083

摘　要：为了更高效处理含砷铜精矿，砷可以通过高温过滤尘土和低温分离冷凝氧化砷 2 个步骤进行提取。焙烧环境中的氧含量对精矿中的残余砷含量有重要影响。当氧含量较高时，形成的砷酸盐残留在精矿中。当氧含量较低时，形成的硫化砷会堵塞滤饼残。在 700 ℃、氧含量为 4%(体积分数)的条件下焙烧，得到精矿的残余砷含量最低，由 11.8%降低到 0.34%(质量分数)。在中试实验中，可通过控制进料速度间接控制氧含量，能将残余砷含量降低到 0.48%(质量分数)，同时，回收的 As_2O_3 纯度可以达到 99.17%(质量分数)。基于砷在不同氧含量下形态变化的机理，提出控氧焙烧与两次过滤的新工艺，并且成功运用于中试，使铜精矿中的残余砷含量低于中国精矿矿物含砷量标准(0.5%(质量分数))。

关键词：砷；含砷铜精矿；过滤；焙烧；多孔材料

(Edited by Bing YANG)